The Astrophysical Journal, 934:87 (7pp), 2022 July 20 https://doi.org/10.3847/1538-4357/ac7b2c

A Massive, Dusty, HI Absorption–Selected Galaxy at $z \approx 2.46$ Identified in a CO Emission Survey

B. Kaur[1], N. Kanekar[1], M. Revalski[2], M. Rafelski[2,3], M. Neeleman[4], J. X. Prochaska[5,6], and F. Walter[4]
[1] National Centre for Radio Astrophysics, Tata Institute of Fundamental Research, Pune University, Pune 411007, India; bkaur@ncra.tifr.res.in
[2] Space Telescope Science Institute, 3700 San Martin Drive, Baltimore, MD 21218, USA
[3] Department of Physics & Astronomy, Johns Hopkins University, Baltimore, MD 21218, USA
[4] Max-Planck-Institut für Astronomie, Königstuhl 17, D-69117, Heidelberg, Germany
[5] Department of Astronomy & Astrophysics, UCO/Lick Observatory, University of California, 1156 High Street, Santa Cruz, CA 95064, USA
[6] Kavli Institute for the Physics and Mathematics of the Universe (Kavli IPMU), 5-1-5 Kashiwanoha, Kashiwa, 277-8583, Japan
Received 2022 May 13; revised 2022 June 15; accepted 2022 June 17; published 2022 July 27

Abstract

We report a NOrthern Extended Millimeter Array (NOEMA) and Atacama Large Millimeter/submillimeter Array search for redshifted CO emission from the galaxies associated with seven high-metallicity ($[M/H] \geqslant -1.03$) damped Lyα absorbers (DLAs) at $z \approx 1.64$–2.51. Our observations yielded one new detection of CO(3–2) emission from a galaxy at $z = 2.4604$ using NOEMA, associated with the $z = 2.4628$ DLA toward QSO B0201+365. Including previous searches, our search results in detection rates of CO emission of $\approx 56^{+38}_{-24}\%$ and $\approx 11^{+26}_{-9}\%$, respectively, in the fields of DLAs with $[M/H] > -0.3$ and $[M/H] < -0.3$. Further, the HI–selected galaxies associated with five DLAs with $[M/H] > -0.3$ all have high molecular gas masses, $\gtrsim 5 \times 10^{10}\, M_\odot$. This indicates that the highest-metallicity DLAs at $z \approx 2$ are associated with the most massive galaxies. The newly identified $z \approx 2.4604$ HI–selected galaxy, DLA0201+365g, has an impact parameter of ≈ 7 kpc to the QSO sightline, and an implied molecular gas mass of $(5.04 \pm 0.78) \times 10^{10} \times (\alpha_{CO}/4.36) \times (r_{31}/0.55)\, M_\odot$. Archival Hubble Space Telescope Wide Field and Planetary Camera 2 imaging covering the rest-frame near-ultraviolet (NUV) and far-ultraviolet (FUV) emission from this galaxy yield nondetections of rest-frame NUV and FUV emission, and a 5σ upper limit of $2.3\, M_\odot\ \mathrm{yr}^{-1}$ on the unobscured star formation rate (SFR). The low NUV-based SFR estimate, despite the very high molecular gas mass, indicates that DLA0201+365g either is a very dusty galaxy, or has a molecular gas depletion time that is around 2 orders of magnitude larger than that of star-forming galaxies at similar redshifts.

Unified Astronomy Thesaurus concepts: High-redshift galaxies (734); Damped Lyman-alpha systems (349); CO line emission (262)

1. Introduction

The highest HI column density absorbers in QSO absorption spectra, the damped Lyα absorbers (DLAs, with $N(HI) \geqslant 2 \times 10^{20}\ \mathrm{cm}^{-2}$; Wolfe et al. 1986) are expected to arise in gas associated with galaxies (e.g., Wolfe et al. 2005). The presence of a DLA in a quasar spectrum thus allows one to identify high-z galaxies via their Lyα absorption signature, rather than via their luminosity. Such HI absorption–selected galaxies do not have the luminosity bias that affects emission-selected samples, making them complementary probes of galaxy evolution that are sensitive to galaxies with effectively any mass.

Many attempts have been made, mostly at optical and near-IR wavelengths, to identify and characterize high-z HI absorption–selected galaxies, and thereby establish their connection to the emission-selected population (e.g., Warren et al. 2001; Kulkarni et al. 2006; Péroux et al. 2011; Fumagalli et al. 2015; Krogager et al. 2017; Mackenzie et al. 2019). A number of these studies (e.g., Møller et al. 2004; Fynbo et al. 2010; Wang et al. 2015) have focused on DLAs with high absorption metallicities, as the correlation between DLA metallicities and the velocity widths of the low-ionization metal lines suggests the existence of a mass–metallicity relation in DLAs (e.g., Ledoux et al. 2006; Prochaska et al. 2008; Neeleman et al. 2013). However, the presence of the background quasar, which is very bright at these wavelengths relative to the foreground galaxy, has been a significant hindrance to these efforts. As a result, only ≈20 HI–selected galaxies have been identified via such studies at high redshifts, $z \gtrsim 2$ (e.g., Møller et al. 2004; Fynbo et al. 2013; Krogager et al. 2017; Mackenzie et al. 2019; Ranjan et al. 2020).

In the last few years, with the advent of the Atacama Large Millimeter/submillimeter Array (ALMA), redshifted CO rotational and [C II] 158 μm fine-structure emission lines have emerged as promising tools to identify and characterize HI–selected galaxies at high redshifts (Neeleman et al. 2016, 2017, 2019; Péroux et al. 2019; Klitsch et al. 2019; Kanekar et al. 2018, 2020; Kaur et al. 2021), yielding a number of surprises. For example, HI–selected galaxies at $z \approx 4$ identified by their [C II] 158 μm emission have large impact parameters, $b \approx 16$–45 kpc, from the QSO sightline (Neeleman et al. 2017, 2019), far larger than expected for sightlines that pass through the interstellar medium of galaxies. This indicates that the DLA sightlines significantly traverse the circumgalactic medium (CGM), with high HI column densities present in the CGM of high-z galaxies. One of the [C II] 158 μm emitters at $z \approx 4.26$ has been shown to be a massive, rotating disk galaxy, the first such cold disk to be identified at $z \gtrsim 4$ (Neeleman et al. 2020). At $z \approx 2$, ALMA CO searches have found evidence that a number of HI–selected galaxies associated with high-

Table 1
Observational Details and Results

QSO	z_{QSO}	z_{DLA}	CO line	ν_{obs} (GHz)	Time (hr)	Beam ($'' \times ''$)	δV (km s^{-1})	RMS$_{CO}$ (μJy/Bm)	$\int S_{CO}\,\delta V$ (Jy km s^{-1})	L'_{CO} (10^9 K km s^{-1} pc^2)
J0927+5823	1.91	1.6352	2–1	87.49	4.0	2.0×1.6	200	173	<0.11	<4.0
J1049−0110[a]	2.12	1.6577	3–2	130.11	1.5	2.3×1.9	200	77	<0.049	<0.81
J1310+5424	1.93	1.8006	2–1	82.32	4.1	3.8×2.7	200	215	<0.14	<5.9
J1417+4132	2.02	1.9509	2–1	78.13	9.0	2.5×1.6	200	184	<0.12	<5.8
J1555+4800	3.30	2.3911	3–2	101.97	4.5	2.9×2.3	200	198	<0.13	<4.0
B0201+365	2.91	2.4628	3–2	99.86	3.4	1.8×1.2	25	500	0.182 ± 0.028	6.36 ± 0.98
J1610+4724	3.22	2.5066	3–2	98.61	7.1	2.3×1.7	200	130	<0.083	<2.8

Notes. The columns are (1) the QSO name, (2) the QSO redshift, (3) the DLA redshift, (4) the observed CO rotational transition, (5) the redshifted CO line frequency in GHz, (6) the on-source time in hours, (7) the synthesized beam in arcseconds, (8) the velocity resolution of the CO spectral cube used for the search in kilometers per second, (9) the rms noise on the cube, in μJy/Bm, (10) the integrated CO line flux density, or the 3σ upper limit to this quantity, assuming a boxcar profile with a width of 200 km s^{-1}, and (11) the CO(2–1) or CO(3–2) line luminosity, L'_{CO}, or the 3σ upper limit to this quantity.
[a] J1049−0110 was observed with ALMA, while the remaining six targets were observed with NOEMA.

metallicity DLAs have both remarkably large molecular gas masses, $\gtrsim 5 \times 10^{10}$ M$_\odot$, and a range of impact parameters, $b \approx 6$–100 kpc (Neeleman et al. 2018; Fynbo et al. 2018; Kanekar et al. 2020). Follow-up multiline CO studies have found evidence for highly excited mid-J CO rotational levels in three of the CO-emitting, HI–selected galaxies at $z \approx 2$ (Klitsch et al. 2022; Kaur et al. 2022).

The very large molecular gas masses of the HI–selected galaxies at $z \approx 2$ is an especially surprising result of the ALMA CO and [C II] 158 μm studies. However, the number of absorber fields at $z \approx 2$ that have been searched for CO emission remains quite small, with 5 CO detections in 12 searches so far (Kanekar et al. 2020). The recent upgrade of the NOrthern Extended Millimeter Array (NOEMA) has opened the possibility of carrying out such searches for redshifted CO emission from HI–selected galaxies at northern declinations, i.e., those inaccessible to ALMA. In this paper, we report a NOEMA and ALMA search for redshifted CO(2–1) or CO(3–2) emission from the fields of seven high-metallicity DLAs at $z \approx 2$, with absorption metallicity $[\mathrm{M/H}] \gtrsim -1.0$, which has resulted in one new CO detection, in the field of the $z \approx 2.4628$ DLA toward QSO B0201+365. We also report a search for rest-frame far-ultraviolet (FUV) and near-ultraviolet (NUV) emission from the new HI–selected galaxy, using Hubble Space Telescope (HST) Wide Field and Planetary Camera 2 (WFPC2) archival data.

2. Observations, Data Analysis, and Results

2.1. NOEMA and ALMA Observations

We used NOEMA and ALMA to carry out a search for redshifted CO(2–1) or CO(3–2) emission in the fields of seven DLAs at $z \approx 1.64$–2.51. The targeted DLAs have an absorption metallicity, $[\mathrm{M/H}] \geqslant -1.03$, higher than the median DLA metallicity (≈ -1.3; Rafelski et al. 2014) in this redshift range. Six of the DLAs were observed with the NOEMA Band-1 receivers between December 2017 and April 2018 (project: W17DG; PI: M. Neeleman), in the D configuration. The PolyFix correlator was used as the backend, with an instantaneous bandwidth of 8 GHz centered on the redshifted CO(2–1) or CO(3–2) frequency of the target DLA, and subdivided into 4000 channels, giving a frequency resolution of 2 MHz. The seventh DLA was observed with the ALMA Band-4 receivers (proposal: 2016.1.00628.S; PI: J. X. Prochaska) in January 2017. One of the 1.875 MHz intermediate frequency (IF) bands was used in Frequency Division Mode (FDM) mode to cover the redshifted CO(3–2) line frequency, with 480 channels and a spectral resolution of 3.9 MHz, while the remaining three IF bands used the Time Division Mode (TDM) mode, with a 2 GHz bandwidth and 128 channels, to cover the continuum emission. The on-source times were 4–9 hr (NOEMA) and 1.5 hr (ALMA). We note that the FWHMs of the NOEMA and ALMA fields of view at the redshifted CO line frequencies are $\gtrsim 50''$, corresponding to a spatial field of view of $\gtrsim 400$ kpc at the DLA redshifts.[7] The observational details are summarized in Table 1.

The initial editing and calibration were carried out in GILDAS[8] for the NOEMA data, and with the standard ALMA pipeline in the Common Astronomy Software Applications package (CASA version 5.6; McMullin et al. 2007) for the ALMA data. Only one of the seven QSOs, QSO B0201+365, had a sufficient flux density ($\approx$31 mJy) for self-calibration; this was carried out in the Astronomical Image Processing System package ("classic" AIPS; Greisen 2003), following standard procedures. Any detected continuum emission in each field was then subtracted out from the calibrated spectral-line visibilities, after Fourier-transforming the continuum image to the visibility plane. The residual spectral-line visibilities were then imaged in CASA, using the task TCLEAN to produce spectral cubes at velocity resolutions of 25–200 km s^{-1}. The cubes were then visually inspected to search for redshifted CO(2–1) or CO(3–2) emission.

We detect CO(3–2) emission from one galaxy (hereafter, DLA0201+365g, at R.A. = $02^h04^m55^s.55$, decl. = $+36°49'17''.3$, $z = 2.4604$) in the field of the $z = 2.4628$ DLA toward QSO B0201+365. Panels (a) and (b) of Figure 1 show the velocity-integrated CO(3–2) moment-0 image and the CO(3–2) spectrum, the latter obtained from a cut through the peak position of the velocity-integrated image. Both the image and the spectrum show clear detections of the CO(3–2) emission line, at $\approx 6.5\sigma$ statistical significance. We obtain a velocity-integrated CO(3–2) line flux density of (0.182 ± 0.028) Jy km s^{-1}, implying a CO(3–2) line luminosity of $L'_{CO(3-2)} = (6.36 \pm 0.98) \times 10^9$ K km s^{-1} pc^2. The CO line FWHM is $\approx$125 km s^{-1}, and the impact parameter to the QSO sightline is $\approx 0''.89$, i.e., $\approx$7 kpc at $z = 2.4628$.

No statistically significant ($\geqslant 5\sigma$) emission was detected in the fields of the remaining six DLAs, at or near the redshifted

[7] Throughout the paper, we use a Λ-CDM cosmology, assuming $\Omega_\Lambda = 0.685$, $\Omega_m = 0.315$, and $H_0 = 67.4$ km s^{-1} Mpc^{-1} (Planck Collaboration 2020).
[8] https://www.iram.fr/IRAMFR/GILDAS

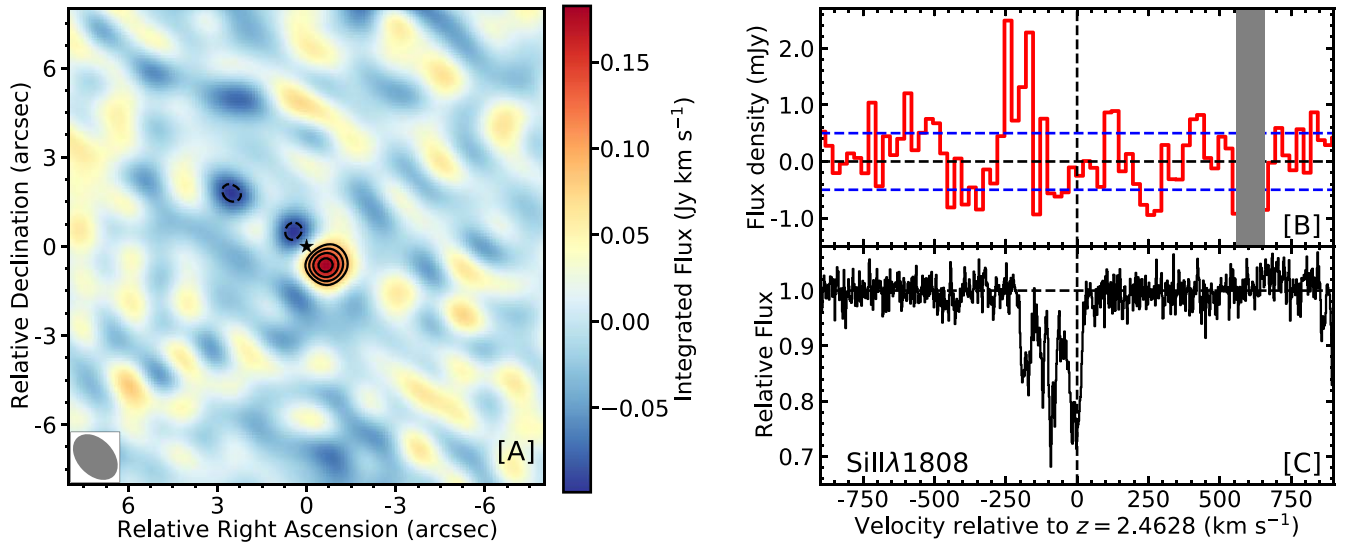

Figure 1. (a) The NOEMA CO(3–2) emission from the HI–selected galaxy in the field of the $z = 2.4628$ DLA toward QSO B0201+365. The contours are at (−4.0, −3.0, 3.0, 4.0, 5.0, 6.0) × σ significance, with dashed negative contours; note that there are no -4σ contours in the image. The axes are relative to the QSO position, indicated by the black star. We note that the $\approx 3\sigma$ negatives in the image are not aligned with the dirty beam. (b) The NOEMA CO(3–2) emission spectrum of DLA0201+365g, obtained by taking a cut through the CO cube at the location of the peak in (a). The blue lines represent the $\pm 1\sigma$ error on the spectrum. The vertical gray band indicates channels in the NOEMA frequency coverage that were masked out due to systematic effects. These channels have systematically lower visibilities compared to other channels; the origin of this effect is not known. (c) The SiIIλ1808 Å absorption line, from the Keck-HIRES spectrum of Prochaska & Wolfe (1996). In both (b) and (c), the velocity is plotted relative to the redshift of the strongest absorption component, $z = 2.4628$.

CO line frequency. The 3σ upper limits on the velocity-integrated CO(3–2) or CO(2–1) line flux densities are (0.05–0.14) Jy km s^{-1}, assuming a line FWHM of 200 km s^{-1}, all below the detection for DLA0201+365g. The corresponding 3σ upper limits on the CO(2–1) or CO(3–2) line luminosities are listed in the last column of Table 1.

2.2. HST-WFPC2 Data

The field of QSO B0201+365 was observed with HST-WFPC2 in 1999 October with the F450W and F814W filters (program ID: 8085; PI: S. Beckwith). The two filters cover, respectively, the rest-frame FUV and NUV emission from the $z = 2.4604$ HI–selected galaxy, with two exposures in a single orbit in each filter. After removing cosmic rays with a custom application[9] of LACOSMIC (van Dokkum 2001), the individual exposures in each filter were combined with DRIZZLEPAC (Hack et al. 2020). Specifically, the HST images were aligned with TWEAKREG using the Gaia DR3 catalog as the astrometric reference (Gaia Collaboration 2021). The routine ASTRODRIZZLE was used to drizzle the combined images, with a final pixel fraction of 1 at a pixel scale of 0.0996″/pixel.

Since DLA0201+365g is located close to one of the diffraction spikes of the QSO point-spread function (PSF); subtraction of the QSO PSF is critical to detect the faint galaxy. The QSO PSF was subtracted using a PSF model obtained from stacking four stars (using a custom code hst_wfc3_psf_modeling[10]) on the same detector chip as the QSO, and separately, from a PSF model obtained by rotating the QSO itself by 180°; similar results were obtained from the two approaches. In the following, we use results from the latter approach.

Figure 2 shows overlays of the NOEMA CO(3–2) emission from DLA0201+365g on the HST-WFPC2 F450W and F814W images. We detect no statistically significant emission in the HST images at the location of DLA0201+365g, with 5σ upper limits of $m_{AB} < 24.9$ in the F450W filter and $m_{AB} < 25.7$ in the F814W filter, corresponding to the rest-frame FUV and NUV wavelengths for DLA0201+365g, respectively. Assuming a Kroupa initial mass function (Kroupa 2001) and the star formation rate (SFR) calibration of Kennicutt & Evans (2012), we obtain 5σ upper limits on the unobscured SFR of $<4.9\,M_\odot$ yr^{-1} (FUV) and <2.3 M$_\odot$ yr^{-1} (NUV).

3. Discussion

Our new NOEMA and ALMA CO searches have yielded one detection of redshifted CO emission from the HI–selected galaxy DLA0201+365g in the field of the $z = 2.4628$ DLA toward QSO B0201+365, and six nondetections of CO emission in the fields of the other DLAs. The measured CO line luminosities of Table 1 can be converted to molecular gas masses via the relation, $M_{\rm mol} = \alpha_{\rm CO} \times {\rm r_{J1}} \times L'_{\rm CO(J\rightarrow J-1)}$, where $\alpha_{\rm CO}$ is the CO-to-H_2 conversion factor (e.g., Bolatto et al. 2013) and ${\rm r_{J1}} \equiv L'_{\rm CO(J\rightarrow J-1)}/L'_{\rm CO(1-0)}$ is the ratio of CO(J → J − 1) and CO(1 − 0) line luminosities (e.g., Carilli & Walter 2013). The value of of $\alpha_{\rm CO}$ depends on physical conditions in the gas, including temperature, density, and metallicity (Bolatto et al. 2013; Carilli & Walter 2013; Tacconi et al. 2020). Following Kanekar et al. (2020), we assume $\alpha_{\rm CO} = 4.36\,M_\odot\,({\rm K\,km\,s^{-1}\,pc^2})^{-1}$ for all targets, a reasonable assumption for nonstarburst galaxies with near-solar metallicity. We further assume subthermal excitation of the $J = 2$ and $J = 3$ rotational levels, with ${\rm r_{21}} = 0.77$ and ${\rm r_{31}} = 0.55$, applicable to high-z main-sequence galaxies (Daddi et al. 2015; Tacconi et al. 2020). In the case of DLA0201+365g, we obtain a high molecular gas mass of $M_{\rm mol} = (5.04 \pm 0.78) \times ({\rm r_{31}}/0.55) \times (\alpha_{\rm CO}/4.36) \times 10^{10}\,M_\odot$. For the CO nondetections in the six DLA fields, our upper limits on the CO(2–1) or CO(3–2) line luminosity yield 3σ upper limits of $M_{\rm mol} < (0.6 - 3.3) \times 10^{10}\,M_\odot$ on the molecular gas mass of the HI–selected galaxies

[9] https://github.com/mrevalski/hst_wfc3_lacosmic
[10] https://github.com/mrevalski/hst_wfc3_psf_modeling

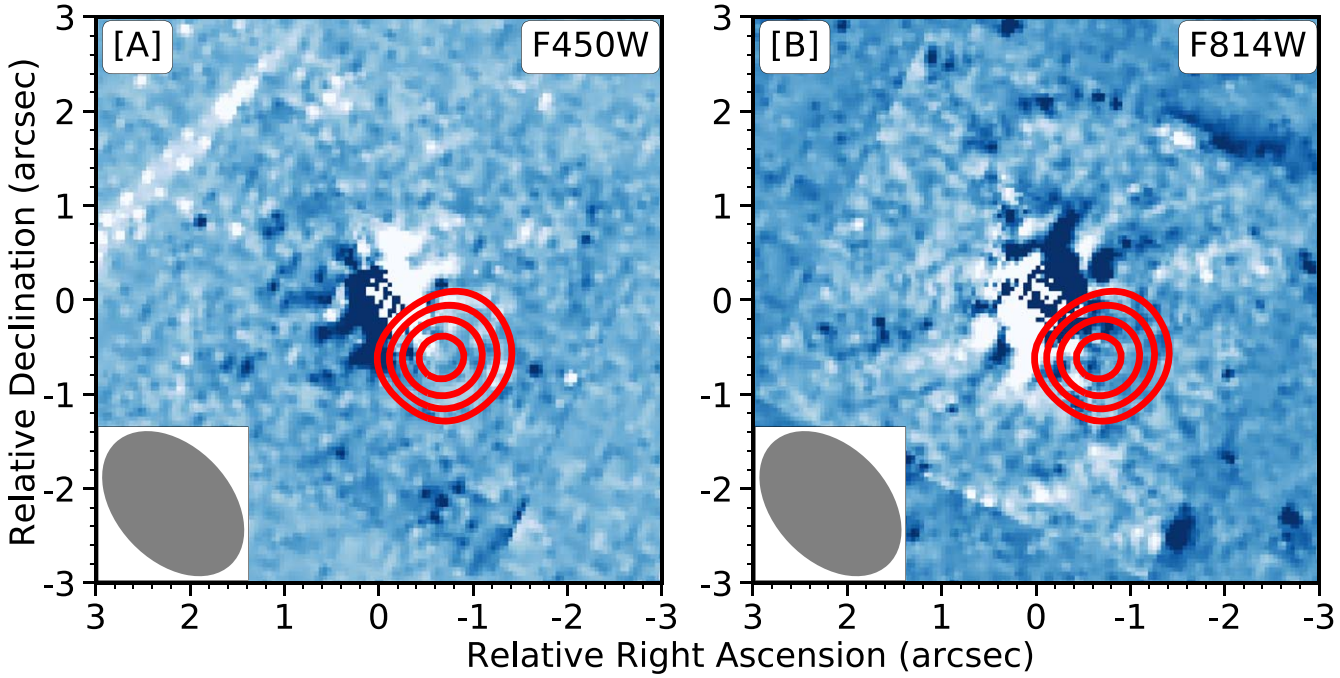

Figure 2. The figure shows the HST-WFPC2 (a) F450W and [B] F814W images (in color) of the field of QSO B0201+365, after subtracting the QSO PSF. The NOEMA velocity-integrated CO(3–2) emission is overlaid (in red contours) on the two HST-WFPC2 images. No emission can be seen in the HST-WFPC2 images at the location of the CO emission.

Table 2
Absorption Properties of the Seven DLAs, and Emission Properties of the Associated HI–Selected Galaxies

QSO	z_{abs}	$\log(N_{HI}/cm^{-2})$	[M/H]	ΔV_{90} (km s^{-1})	$L'_{CO(1-0)}$ (10^9 K km s^{-1} pc^2)	M_{mol} ($\times 10^{10}$ $M_\odot$)	References
J0927+5823	1.6352	20.40 ± 0.15	+0.06	208	<5.14	<2.24	(1)
J1049–0110	1.6577	21.35 ± 0.15	−1.03	330	<0.15	<0.64	(1)
J1310+5424	1.8006	21.45 ± 0.15	−0.52	86	<7.62	<3.32	(1)
J1417+4132	1.9509	21.85 ± 0.15	−0.93	114	<7.52	<3.28	(1)
J1555+4800	2.3911	21.50 ± 0.15	−0.46	199	<7.19	<3.14	(1)
B0201+365	2.4628	20.38 ± 0.04	−0.24	200	11.6 ± 1.8	5.04 ± 0.78	(2, 3)
J1610+4724	2.5066	21.00 ± 0.15	−0.35	155	<5.12	<2.23	(1)

Note. The columns are (1) the QSO name, (2) the DLA redshift, (3) the logarithm of the HI column density (in per centimeters squared), (4) the absorption metallicity, [M/H], (5) the velocity spread of the low-ionization metal lines, ΔV_{90}, in kilometers per second, (6) the CO(1–0) line luminosity or the 3σ upper limit to this quantity, in 10^9 K km s^{-1} pc^2, assuming $r_{21} = 0.77$ and $r_{31} = 0.55$ (Tacconi et al. 2020), (7) the molecular gas mass of the HI–selected galaxy, or the 3σ upper limit to this quantity, in 10^{10} $M_\odot$, and (8) references for the DLA absorption properties.
References: (1) Berg et al. (2015), (2) Prochaska & Wolfe (1996), (3) Neeleman et al. (2013).

associated with the DLAs. Table 2 summarizes the absorption and emission properties of the DLAs and the HI–selected galaxies.

We note that Klitsch et al. (2022) find tentative evidence for a lower α_{CO} value in two of the $z \approx 2$ HI–selected galaxies of the sample of Kanekar et al. (2020), at $z \approx 2.1929$ toward PKS B1228-113 and $z \approx 2.5832$ toward QSO J0918+1636. These two galaxies also show near-thermal excitation of the J = 3 rotational level (Kaur et al. 2022). However, these galaxies have the highest measured CO(3–2) line luminosities of the sample, and it is not clear whether their properties are representative of the full sample. Larger samples are needed to explore the excitation conditions of high-z HI–selected galaxies.

The newly detected HI–selected galaxy DLA0201+365g has a high inferred molecular gas mass, $\approx 5 \times 10^{10} M_\odot$. Remarkably, the CO line FWHM is only $\approx$125 km s^{-1}, significantly smaller than the CO FWHMs ($\gtrsim$300 km s^{-1}; Kanekar et al. 2020) of the other HI–selected galaxies at $z \approx 2$ with CO detections. This suggests that DLA0201+365g has a low inclination to our line of sight. Conversely, the low-ionization metal absorption lines are both wide, $\Delta V_{90} \approx 200$ km s^{-1} (Prochaska & Wolfe 1996; Neeleman et al. 2013), and asymmetric, with the strongest SiIIλ1808 Å absorption of Figure 1(C) seen to lie at one edge of the line, $\approx$200 km s^{-1}, redward of the CO emission. It is not straightforward to reconcile the narrow observed CO emission with the wide metal absorption lines. One possibility is that the CO emission is detected only from the central regions of the galaxy, which may have higher excitation of the mid-J CO rotational levels, yielding stronger CO(3–2) emission. Alternatively, part of the low-ionization metal line absorption may arise in dense clumps in the CGM of the HI–selected galaxy, or possibly in a companion galaxy not detected in CO emission.

Our nondetection of DLA0201+365g in the HST-WFPC2 F814W image of Figure 2, covering its rest-frame NUV emission, implies an upper limit of 2.3 $M_\odot$ yr^{-1} on the unobscured SFR of

the HI–selected galaxy. Wang et al. (2015) used the Gemini Near-Infrared Integral Field Spectrometer (NIFS) to search for redshifted Hα emission from galaxies in the field of the 2.4628 DLA, reporting a nondetection of Hα emission. We reinspected the Gemini-NIFS Hα cube at the spatial position of the CO emission, and found no evidence for Hα emission at the position of the CO emission. The Hα nondetection places the 3σ upper limit of $\approx 2.2\ M_{\odot}\ \mathrm{yr}^{-1}$ on the SFR of DLA0201+365g (Wang et al. 2015), similar to the SFR limit from the nondetection of rest-frame NUV emission. We emphasize that these limits are on the dust-unobscured SFR, as any dust obscuration would attenuate the rest-frame NUV and the Hα emission.

Combining our molecular gas mass estimate with the upper limit on the rest-frame NUV SFR allows us to estimate the molecular gas depletion timescale, $t_{\rm dep} \equiv M_{\rm mol}/\mathrm{SFR}$, of DLA0201+365g. This is the timescale on which all the molecular gas of a galaxy would be converted to stars at its current SFR, assuming no replenishment of the gas reservoir. We obtain $t_{\rm dep} > 22$ Gyr for DLA0201+365g (>15 Gyr, on including the 2σ uncertainty in the molecular gas mass), more than 1 order of magnitude larger than the molecular gas depletion timescales in star-forming galaxies at $z \approx 2.5$ (e.g., Tacconi et al. 2020) or in the local universe (e.g., Saintonge et al. 2017).

Large molecular gas depletion timescales (3–120 Gyr) have also been found in HI–selected galaxies at intermediate redshifts, $z \approx 0.5$–0.8 (Møller et al. 2018; Kanekar et al. 2018). However, in at least one case here, the $z \approx 0.7163$ HI–selected galaxy J1323-0021g, the dust-obscured SFR, estimated from the Herschel image, is ≈3 times higher than the SFR estimate from the Hα line (Møller et al. 2018). This implies a significantly lower molecular gas depletion time, ≈5 Gyr, when obscuration effects are taken into account.

Similar to the $z \approx 0.7163$ HI–selected galaxy, J1323-0021g, a more plausible explanation of the low NUV and Hα SFR estimates in DLA0201+365g is dust obscuration of the NUV and Hα emission. An independent estimate of the total SFR may be obtained from the typical molecular gas depletion timescales of star-forming galaxies at the DLA redshift. We estimate $t_{\rm dep} \approx 0.22$ Gyr for DLA0201+365g from the median of measurements of $t_{\rm dep}$ in star-forming galaxies at $z \approx 2.46$ (Tacconi et al. 2020). Combining this with the molecular gas mass estimate of $5.04 \times 10^{10}\ M_{\odot}$ gives a total SFR of $\approx 230\ M_{\odot}\ \mathrm{yr}^{-1}$, 2 orders of magnitude larger than the upper limits on the SFR from the rest-frame NUV and Hα nondetections. We note that even a molecular gas depletion time of ≈1–2 Gyr, similar to that of galaxies in the local universe (e.g., Leroy et al. 2013; Saintonge et al. 2017), would yield a total SFR of $\approx 50\ M_{\odot}\ \mathrm{yr}^{-1}$. This suggests that DLA0201 is likely to be a very dusty galaxy.

The ratio of the Zn abundance to the Fe (or Cr) abundance in DLAs has been used to quantify the extent of depletion of refractory elements onto dust grains (e.g., Pettini et al. 1994, 1997; Hou et al. 2001; Prochaska & Wolfe 2002; Ledoux et al. 2003; De Cia et al. 2016), although challenges exist such as observations showing that Zn traces S (Fenner et al. 2004; Rafelski et al. 2012; Roman-Duval et al. 2022). Specifically, we note that there are caveats in using [Zn/Fe] as a dust indicator, as the origins of Zn are uncertain and the Zn abundance also depends on the star formation history of a galaxy (e.g., Fenner et al. 2004). Regardless, Roman-Duval et al. (2022) find that [Zn/Fe] generally traces the depletion of heavy elements in DLAs. For DLA0201+365, [Zn/Fe] = +0.58 (Prochaska et al. 2007), indicating that the DLA sightline is dusty, with substantial Fe depletion. This is broadly consistent with the result that DLA0201+365g is a dusty galaxy. The depletion in DLA0201+365 is similar to that in the other $z \approx 2$ DLAs that show CO emission from the associated galaxies (Kanekar et al. 2020). Five of the six DLAs have [Zn/Fe] (or [Zn/Cr]) in the range +0.58 to +0.91. DLA2225+0527 is the only absorber of the sample with a significantly higher depletion, [Zn/Fe] = +1.23; here, the background QSO shows significant dust reddening (Krogager et al. 2016).

The sample of $z \approx 2$ DLAs with searches for redshifted CO emission consists of 19 systems, with 6 CO detections and 13 nondetections (Neeleman et al. 2018; Fynbo et al. 2018; Kanekar et al. 2020, this work), i.e., a CO detection rate of ≈32%. All 19 DLAs have absorption metallicities $\geqslant -1.03$, i.e., higher than the median DLA metallicity (≈−1.3; Rafelski et al. 2014) in this redshift range. Figure 3 plots the measured or inferred CO(1–0) line luminosity of the HI–selected galaxies against the absorption metallicity of the corresponding DLAs. The figure shows that a transition from a high CO detection rate to a low detection rate appears to take place at the metallicity $[\mathrm{M/H}] \approx -0.3$, indicated by the dashed vertical line. Five of the nine DLAs with $[\mathrm{M/H}] > -0.3$ have detections of CO emission, i.e., a CO detection rate of 56^{+38}_{-24}%, while only one of the nine DLAs with $[\mathrm{M/H}] < -0.3$ shows CO emission, yielding a CO detection rate of $\approx 11^{+26}_{-9}$%. Thus, although the sample remains small, we find evidence for a higher detection rate of CO emission from galaxies associated with high-metallicity DLAs.

Further, all five CO emitters associated with the highest-metallicity DLAs, with $[\mathrm{M/H}] > -0.3$, have high CO line luminosities, $L'_{\mathrm{CO}(1-0)} > 10^{10}\ \mathrm{K\ km\ s^{-1}\ pc^2}$. This suggests that the CO line luminosities of HI–selected galaxies may depend on the absorption metallicity. We tested this hypothesis by carrying out Peto-Prentice and Gehan generalized Wilcoxon tests, using the ASURV package (Feigelson & Nelson 1985), comparing the CO line luminosity distributions of galaxies associated with two subsamples of DLAs, with metallicities above and below $[\mathrm{M/H}] = -0.3$. We find that the null hypothesis, that the two samples are drawn from the same CO line luminosity distribution, is ruled out at $\approx 2.3\sigma$ significance. We thus find evidence that both the CO detection rate and the CO line luminosity are higher in HI–selected galaxies associated with the highest-metallicity DLAs, with $[\mathrm{M/H}] > -0.3$.

4. Summary

We have used NOEMA and ALMA to search for redshifted CO(2–1) or CO(3–2) emission in the fields of seven high-metallicity ($[\mathrm{M/H}] \geqslant -1.03$) DLAs at $z \approx 1.64$–2.51. Our searches yielded one CO detection and six nondetections of CO emission, the latter providing 3σ upper limits of $(0.6\text{–}3.3) \times 10^{10}\ M_{\odot}$ on the molecular gas masses of the associated galaxies. Thus far, including the work presented here, the fields of 19 high-metallicity DLAs at $z \approx 2$ have been searched for CO emission from the associated HI–selected galaxies, with six detections of CO emission, i.e., a CO detection fraction of ≈32%. We find evidence for both a higher CO detection fraction and higher CO line luminosities in HI–selected galaxies associated with the highest-metallicity DLAs, with $[\mathrm{M/H}] > -0.3$. The new NOEMA detection of redshifted CO(3–2) emission is from DLA0201+365g, at $z = 2.4604$, associated with the $z = 2.4628$ DLA toward QSO B0201+365.

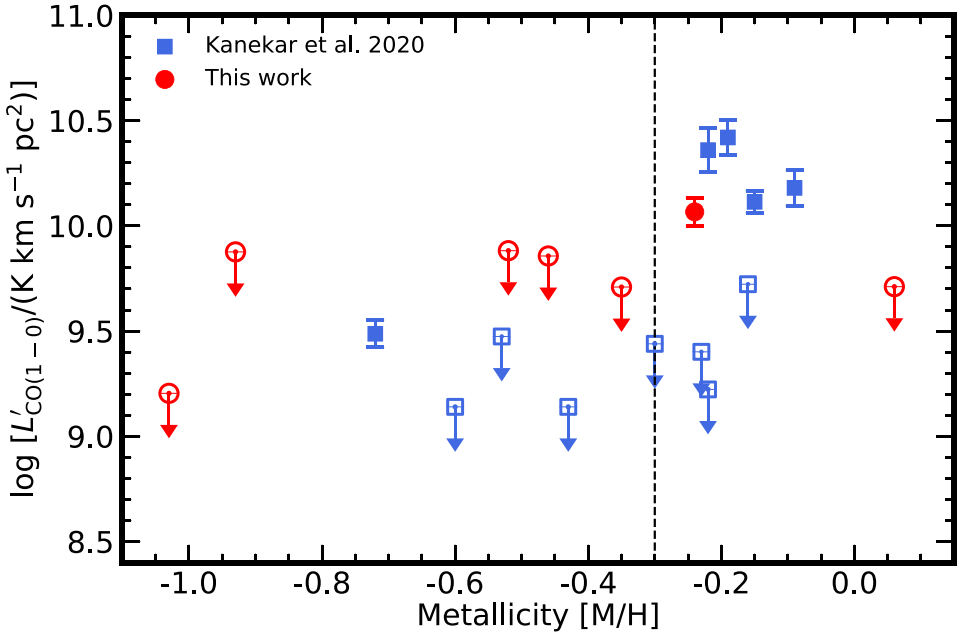

Figure 3. The CO(1–0) line luminosity plotted against the DLA absorption metallicity for the 19 DLAs at $z \approx 2$ with searches for redshifted CO emission. The red circles indicate measurements from the present work, while the blue squares show the sample of Kanekar et al. (2020); CO detections and nondetections are shown, respectively, with filled and open symbols, the latter with downward-pointing arrows. For two DLAs, B1228-113 at $z = 2.1929$ and J0918+1636 at $z = 2.5832$, we show the actual measured CO(1–0) line luminosity (Kaur et al. 2022); for the remaining 17 systems, the CO(1–0) line luminosity is inferred from measurements of the CO(2–1), CO(3–2), or CO(4–3) luminosities, assuming subthermal excitation with $r_{21} = 0.77$, $r_{31} = 0.55$, and $r_{41} = 0.42$ (Tacconi et al. 2020). The dashed vertical line indicates the metallicity [M/H] = −0.3, above which we find a higher CO detection fraction, ≈56%.

We obtain a high molecular gas mass, $M_{\rm mol} = (5.04 \pm 0.78) \times 10^{10} \times (\alpha_{\rm CO}/4.36) \times (r_{31}/0.55)\, M_\odot$ for this galaxy. The nondetection of rest-frame FUV and NUV emission from DLA0201+365g in HST-WFPC2 images of the field places an upper limit of ≈2.3 $M_\odot$ yr^{-1} on its dust-unobscured SFR, similar to the limit from the earlier nondetection of Hα emission. This would imply that the galaxy has an extremely large molecular gas depletion timescale, $\gtrsim$22 Gyr, more than 1 order of magnitude larger than that of star-forming galaxies at similar redshifts or in the local universe. More plausibly, if the galaxy has a molecular gas depletion timescale similar to that of other galaxies at $z \approx 2.46$, we obtain a total SFR of ≈230 $M_\odot$ yr^{-1}, 2 orders of magnitude higher than the upper limits from the NUV and Hα nondetections, implying that the object would be a very dusty galaxy. The CO emission is significantly narrower than the spread of the low-ionization metal absorption lines suggesting that either the CO emission arises from only the central regions of the galaxy, or a significant fraction of the absorption arises in the CGM.

B.K. and N.K. acknowledge the Department of Atomic Energy for funding support, under project 12-R&D-TFR-5.02-0700. M.N. acknowledges support from ERC advanced grant 740246 (Cosmic_Gas). We thank an anonymous referee for comments on an earlier version of the manuscript, Nichol Cunningham for much help with calibrating the NOEMA data, and Wei-Hao Wang for discussions and for providing us with the analyzed Gemini-NIFS spectral cube. This work is based on observations carried out under project number W17DG [Sep-17] with the IRAM NOEMA Interferometer. IRAM is supported by INSU/CNRS (France), MPG (Germany) and IGN (Spain). This paper makes use of the following ALMA data: ADS/JAO.ALMA#2016.1.00628.S. ALMA is a partnership of ESO (representing its member states), NSF (USA), and NINS (Japan), together with NRC (Canada), MOST and ASIAA (Taiwan), and KASI (Republic of Korea), in cooperation with the Republic of Chile. The Joint ALMA Observatory is operated by ESO, AUI/NRAO and NAOJ. This research is based on observations made with the NASA/ESA Hubble Space Telescope obtained from the Space Telescope Science Institute, which is operated by the Association of Universities for Research in Astronomy, Inc., under NASA contract NAS 526555. These observations are associated with program 8085. This material is based upon work supported by the National Science Foundation under grant No. 2107989.

Software: DrizzlePac (Hack et al. 2020), LACOSMIC (van Dokkum 2001), CASA (v5.6; McMullin et al. 2007), AIPS (Greisen 2003), ASURV (Feigelson & Nelson 1985), ASTROPY (Astropy Collaboration et al. 2013).

ORCID iDs

B. Kaur https://orcid.org/0000-0002-1372-0686
N. Kanekar https://orcid.org/0000-0002-9757-7206
M. Revalski https://orcid.org/0000-0002-4917-7873
M. Rafelski https://orcid.org/0000-0002-9946-4731
M. Neeleman https://orcid.org/0000-0002-9838-8191
J. X. Prochaska https://orcid.org/0000-0002-7738-6875
F. Walter https://orcid.org/0000-0003-4793-7880

References

Astropy Collaboration, Robitaille, T. P., Tollerud, E. J., et al. 2013, A&A, 558, A33
Berg, T. A. M., Neeleman, M., Prochaska, J. X., Ellison, S. L., & Wolfe, A. M. 2015, PASP, 127, 167
Bolatto, A. D., Wolfire, M., & Leroy, A. K. 2013, ARA&A, 51, 207
Carilli, C. L., & Walter, F. 2013, ARA&A, 51, 105
Daddi, E., Dannerbauer, H., Liu, D., et al. 2015, A&A, 577, A46
De Cia, A., Ledoux, C., Mattsson, L., et al. 2016, A&A, 596, A97

Feigelson, E. D., & Nelson, P. I. 1985, ApJ, 293, 192
Fenner, Y., Prochaska, J. X., & Gibson, B. K. 2004, ApJ, 606, 116
Fumagalli, M., O'Meara, J. M., Prochaska, J. X., Rafelski, M., & Kanekar, N. 2015, MNRAS, 446, 3178
Fynbo, J. P. U., Laursen, P., Ledoux, C., et al. 2010, MNRAS, 408, 2128
Fynbo, J. P. U., Geier, S. J., Christensen, L., et al. 2013, MNRAS, 436, 361
Fynbo, J. P. U., Heintz, K. E., Neeleman, M., et al. 2018, MNRAS, 479, 2126
Gaia Collaboration 2021, A&A, 649, A1
Greisen, E. W. 2003, in Astrophysics and Space Science Library, Vol. 285, Information Handling in Astronomy—Historical Vistas, ed. A. Heck (Dordrecht: Kluwer Academic Publishers), 109
Hack, W. J., Cara, M., Sosey, M., et al. 2020, spacetelescope/drizzlepac: Drizzlepac, Zenodo, doi:10.5281/zenodo.3743274
Hou, J. L., Boissier, S., & Prantzos, N. 2001, A&A, 370, 23
Kanekar, N., Prochaska, J., Neeleman, M., et al. 2020, ApJL, 901, L5
Kanekar, N., Prochaska, J. X., Christensen, L., et al. 2018, ApJL, 856, L23
Kaur, B., Kanekar, N., Rafelski, M., et al. 2021, ApJ, 921, 68
Kaur, B., Kanekar, N., Rafelski, M., et al. 2022, ApJL, 933, L42
Kennicutt, R. C., & Evans, N. J. 2012, ARA&A, 50, 531
Klitsch, A., Zwaan, M. A., Péroux, C., et al. 2019, MNRAS, 482, L65
Klitsch, A., Christensen, L., Valentino, F., et al. 2022, MNRAS, 514, 2346
Krogager, J. K., Fynbo, J. P. U., Noterdaeme, P., et al. 2016, MNRAS, 455, 2698
Krogager, J. K., Møller, P., Fynbo, J. P. U., & Noterdaeme, P. 2017, MNRAS, 469, 2959
Kroupa, P. 2001, MNRAS, 322, 231
Kulkarni, V. P., Woodgate, B. E., York, D. G., et al. 2006, ApJ, 636, 30
Ledoux, C., Petitjean, P., Fynbo, J. P. U., Møller, P., & Srianand, R. 2006, A&A, 457, 71
Ledoux, C., Petitjean, P., & Srianand, R. 2003, MNRAS, 346, 209
Leroy, A. K., Walter, F., Sandstrom, K., et al. 2013, AJ, 146, 19
Mackenzie, R., Fumagalli, M., Theuns, T., et al. 2019, MNRAS, 487, 5070
McMullin, J. P., Waters, B., Schiebel, D., Young, W., & Golap, K. 2007, in ASP Conf. Ser., 376, Astronomical Data Analysis Software and Systems XVI, ed. R. A. Shaw, F. Hill, & D. J. Bell (San Francisco, CA: ASP), 127
Møller, P., Fynbo, J. P. U., & Fall, S. M. 2004, A&A, 422, L33
Møller, P., Christensen, L., Zwaan, M. A., et al. 2018, MNRAS, 474, 4039
Neeleman, M., Kanekar, N., Prochaska, J. X., et al. 2018, ApJL, 856, L12
Neeleman, M., Kanekar, N., Prochaska, J. X., et al. 2017, Sci, 355, 1285
Neeleman, M., Kanekar, N., Prochaska, J. X., Rafelski, M. A., & Carilli, C. L. 2019, ApJL, 870, L19
Neeleman, M., Prochaska, J. X., Nissim, K., & Rafelski, M. 2020, Natur, 581, 269
Neeleman, M., Wolfe, A. M., Prochaska, J. X., & Rafelski, M. 2013, ApJ, 769, 54
Neeleman, M., Prochaska, J. X., Zwaan, M. A., et al. 2016, ApJL, 820, L39
Péroux, C., Bouché, N., Kulkarni, V. P., York, D. G., & Vladilo, G. 2011, MNRAS, 410, 2237
Péroux, C., Zwaan, M. A., Klitsch, A., et al. 2019, MNRAS, 485, 1595
Pettini, M., King, D. L., Smith, L. J., & Hunstead, R. W. 1997, ApJ, 478, 536
Pettini, M., Smith, L. J., Hunstead, R. W., & King, D. L. 1994, ApJ, 426, 79
Planck Collaboration 2020, A&A, 641, A6
Prochaska, J. X., Chen, H.-W., Wolfe, A. M., Dessauges-Zavadsky, M., & Bloom, J. S. 2008, ApJ, 672, 59
Prochaska, J. X., & Wolfe, A. M. 1996, ApJ, 470, 403
Prochaska, J. X., & Wolfe, A. M. 2002, ApJ, 566, 68
Prochaska, J. X., Wolfe, A. M., Howk, J. C., et al. 2007, ApJS, 171, 29
Rafelski, M., Neeleman, M., Fumagalli, M., Wolfe, A. M., & Prochaska, J. X. 2014, ApJL, 782, L29
Rafelski, M., Wolfe, A. M., Prochaska, J. X., Neeleman, M., & Mendez, A. J. 2012, ApJ, 755, 89
Ranjan, A., Noterdaeme, P., Krogager, J. K., et al. 2020, A&A, 633, A125
Roman-Duval, J., Jenkins, E. B., Tchernyshyov, K., et al. 2022, arXiv:2206.03639
Saintonge, A., Catinella, B., Tacconi, L. J., et al. 2017, ApJS, 233, 22
Tacconi, L. J., Genzel, R., & Sternberg, A. 2020, ARA&A, 58, 157
van Dokkum, P. G. 2001, PASP, 113, 1420
Wang, W.-H., Kanekar, N., & Prochaska, J. X. 2015, MNRAS, 448, 2832
Warren, S. J., Møller, P., Fall, S. M., & Jakobsen, P. 2001, MNRAS, 326, 759
Wolfe, A. M., Gawiser, E., & Prochaska, J. X. 2005, ARA&A, 43, 861
Wolfe, A. M., Turnshek, D. A., Smith, H. E., & Cohen, R. D. 1986, ApJS, 61, 249